Optical generation and bottlenecking of nonzero-wave-vector magnons via Er^{3+} centers in antiferromagnetic MnF_2

G. J. Jongerden, A. F. M. Arts, J. I. Dijkhuis, and H. W. de Wijn
Fysisch Laboratorium, Rijksuniversiteit Utrecht, P.O. Box 80.000, 3508 TA Utrecht, The Netherlands
(Received 23 December 1987)

Optical generation and bottlenecking of nonzero-wave-vector magnons in MnF_2 is accomplished by mediation of the excited $^4F_{9/2}(1)$ Kramers doublet of Er^{3+} centers. Following pulsed optical pumping into the upper doublet level, the generation of resonant magnons is manifest via one-magnon relaxation to the lower level in the event the doublet splitting is made to exceed the magnon gap with an external field. This relaxation, in parallel with the slower spin-phonon relaxation, is in turn observed via the time evolution of the luminescence. Upon severe optical pumping, the magnons become imprisoned under bottlenecking conditions by excited Er^{3+} maintained in the lower $^4F_{9/2}(1)$ component, which then may serve as detectors. These experiments allow one to deduce the magnon lifetime, which indicates that spatial diffusion is a major mechanism of removal out of the excited zone. Additionally, the Zeeman effect of the luminescence is investigated, yielding the splittings of the $^4F_{9/2}(1)$ and $^4I_{15/2}(1)$ doublets, and inferring that the Er^{3+} moments occur in eight different orientations in conformity with the magnetic symmetry.

I. INTRODUCTION

The purpose of this paper is to demonstrate the feasibility of generation and bottlenecking of magnons in ordered magnetic systems by optical excitation of centers.[1] Optical generation is accomplished by selective optical pumping into a suitable excited level followed by a resonant emission of magnons in the nonradiative decay to a second excited level lying as close as a distance within the magnon band. The luminescence emanating from the lower excited state then reflects the number of magnons generated. In the event that the optical pumping is made severe, i.e., the magnon generation exceeds the removal of magnons out of the optically excited volume, a nonequilibrium occupation of the resonant magnon modes develops. Furthermore, because the centers remain optically excited as long as the luminescent lifetime, they accumulate in the lower state to such a concentration that the nonequilibrium magnons suffer multiple reabsorption and emission by the two-level scheme prior to decay. This condition of dynamical equilibrium, commonly referred to as a bottleneck, permits to determine the magnon lifetime in a time-resolved experiment provided the metastable concentration and the relevant system parameters are known.

In real systems, optical generation of magnons by decay among excited states is inevitably associated with the production of resonant phonons via direct spin-phonon relaxation. To discern the generation of magnons, therefore, it is desirable to select a magnetic system in which the magnon dispersion exhibits a gap, i.e., a finite amount of energy is required to excite a magnon already at $k=0$. At level separations below the gap the growth of the luminescence following pulsed optical pumping then is entirely due to phonon production, and magnon generation is apparent from an anomalous speeding up as soon as the level separation is made to exceed the gap, such as with an external magnetic field.

A system eminently meeting these requirements is the well-known antiferromagnet MnF_2 ($T_N=67.3$ K) containing Er^{3+} luminescent centers to a small concentration. We will take advantage of the metastable $^4F_{9/2}(1)$ Kramers doublet of Er^{3+}, which has well-resolved luminescent transitions to the $^4I_{15/2}(1)$ ground-state doublet.[2] To determine the external magnetic fields needed to raise the $^4F_{9/2}(1)$ doublet splitting above the $k=0$ magnon gap, we first examine in Sec. III the Zeeman effect of the $^4F_{9/2}(1)$ doublet, and additionally measure the Zeeman effect of the $^4I_{15/2}(1)$ doublet. Then, in Sec. IV, the generation of magnons resonant with the $^4F_{9/2}(1)$ doublet appears to be manifest in the form of a sudden acceleration of the decay within the doublet as soon as its splitting falls within the magnon band. In fact, the decay becomes dominated by the resonant magnons. The relaxation is in turn observed via the luminescence out of the lower component of the doublet, $^4F_{9/2}(1)_-$, given that the optical pumping is into the upper component, $^4F_{9/2}(1)_+$. Next, in Sec. V, it indeed proves feasible to increase the excited-state population to the extent that the magnons generated attain nonequilibrium occupations.

A particular advantage of the present scheme of optical generation is that it, in principle, allows the generation and examination of monochromatic nonequilibrium magnons throughout the entire Brillouin zone simply by adjusting the level separation of the center. In this sense they bear resemblance to the optical schemes employed in the study of phonons,[3] where, especially in the case of Cr^{3+} in Al_2O_3, a treasure of information has been uncovered regarding the dynamics of high-frequency phonons.[4]

II. EXPERIMENTAL

Selective excitation of the $^4F_{9/2}$ levels of Er^{3+} in MnF_2 was accomplished with an excimer-pumped dye laser, delivering almost linearly polarized light pulses of about 10-ns duration, 0.3-cm^{-1} spectral width, and 100-kW peak power. The specimen, an oriented single crystal of MnF_2:Er^{3+}, was immersed in liquid helium held at 1.5 K. The laser beam, incident along the [001] axis, was focused to a diameter of about 0.2 mm. External magnetic fields of up to 6 T along [001] or [110] were used to make the splitting of the lowest $^4F_{9/2}$ Kramers doublet exceed the magnon energy gap. The inhomogeneity of the field over the sample was 0.02% at maximum. The luminescence around 653 nm, emitted by Er^{3+} at 1.5 K in its return to the $^4I_{15/2}$ ground state, was observed at right angles to the incoming laser beam. The Zeeman components departing from the $^4F_{9/2}(1)$ doublet, whose intensities reflect the populations within the doublet, were selected with an 85-cm grating double monochromator, calibrated with reference to spectral lamps, and having a spectral resolution of 0.004 nm. The light passing the monochromator was detected with a photomultiplier followed by standard photon counting apparatus. The temporal evolutions of the luminescent intensity following each laser pulse were stored in a transient recorder with a minimum sampling time of 20 ns, and subsequently transcribed to a multichannel analyzer for accumulation and further analysis.

For the purpose of the determination of the Zeeman splittings, the precise positions of the relevant components of the $^4F_{9/2}(1)$-$^4I_{15/2}(1)$ transition were determined for each field applied under optical pumping with a cw argon ion laser operating at 514 nm into the broad absorption band associated with the $^4T_1$ state of the Mn^{2+} ions. From $^4T_1$ the energy is efficiently released to Er^{3+} centers acting as traps, resulting in a population of their $^4F_{9/2}$ levels.

The single crystal of MnF_2:Er^{3+} used was grown by use of a Czochralski-pulling technique under a N_2 atmosphere and addition of some $NH_4F{\cdot}HF$ as scavenger. The concentration of Er^{3+} amounts to 0.01 at. % according to atomic absorption spectroscopy. The specimen cut from the boule has the form of a rectangular parallelepiped with dimensions $2.4\times2.0\times12.4$ mm^3. The faces, polished down to 0.1 μm roughness, are perpendicular to [110], [1$\bar{1}$0], and [001], with the longest dimension parallel to [001].

III. ZEEMAN EFFECT OF $^4F_{9/2}(1)$-$^4I_{15/2}(1)$

The Kramers degeneracy of the Er^{3+} doublets is, at 1.5 K, already lifted in the absence of an external field by exchange and dipolar fields originating from neighboring Mn^{2+} ions. This is reflected in the appearance of four clearly resolved lines in the $^4F_{9/2}(1)$-$^4I_{15/2}(1)$ luminescence spectra when pumping into the Mn^{2+} broadbands[2] as well as in the excitation spectra obtained upon monitoring a $^4F_{9/2}(1)$ component. Representative examples of such spectra are shown in Fig. 1. The insets to Fig. 1 provide, over a wider range of wavelengths but with reduced resolution, the luminescence of $^4F_{9/2}(1)$ to the complete $^4I_{15/2}$ multiplet, and, in excitation, the complete $^4F_{9/2}$ multiplet. Unambiguous identification of the various lines associated with the $^4F_{9/2}(1)$-$^4I_{15/2}(1)$ transition may be established from the relative intensities in the excitation spectra, which distinguish between the two $^4I_{15/2}(1)$ states, combined with the temporal developments of the luminescence spectra following pulsed selective excitation, which distinguish between the two $^4F_{9/2}(1)$ states. This identification is mandatory to assign the zero-field splittings of the $^4F_{9/2}(1)$ and $^4I_{15/2}(1)$ doublets, which are found to amount to 1.39 ± 0.03 and 2.71 ± 0.03 cm^{-1}, respectively. Additional weak lines, which become more pronounced the higher the doping of the samples, occur at the long-wavelength side of the luminescence spectrum, but are absent from the excitation spectra. This is indicative of these lines to originate from other centers, presumably dimers of Er^{3+}. It is noted that dimer formation at low concentrations has been observed in other systems.[5]

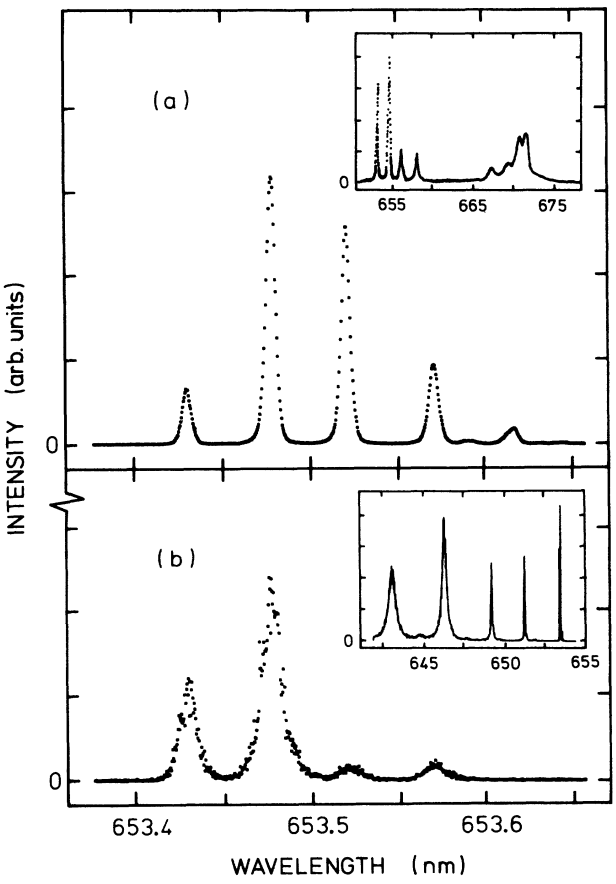

FIG. 1. Spectra of the $^4F_{9/2}(1)$-$^4I_{15/2}(1)$ transition at 1.5 K in zero external field: (a) luminescence spectrum upon excitation at 514 nm; (b) excitation spectrum while monitoring the luminescence of $^4F_{9/2}(1)_-$. Insets show the complete luminescence of $^4F_{9/2}(1)$ to $^4I_{15/2}$, and in excitation the complete $^4F_{9/2}$ multiplet.

The internal fields the Er^{3+} experience along [001] are staggered with the sublattices. In an external magnetic field along [001], therefore, the Er^{3+} ions residing on the

two sublattices become nonequivalent. The net field is increased for Er^{3+} on one sublattice, but decreased for Er^{3+} on the other sublattice. Already in external fields as low as 0.3 T, each of the four luminescent lines of Fig. 1(a) appears in duplicate, as shown in Fig. 2(a). The fact that the two four-line sets are univocally associated with Er^{3+} on the up or down sublattice is best proved by selective excitation, which favors either set depending on the transition chosen for the excitation [Figs. 2(b) and 2(c)]. The complete absence of one set upon excitation of the other further indicates excitation transfer between Er^{3+} on different sublattices not to take place within, say, five times the radiative lifetime, or 1 ms. The Zeeman splitting Δ of the $^4F_{9/2}(1)$ doublet derived from the line separations is presented in the upper panel of Fig. 3. The $^4F_{9/2}(1)$ splitting of Er^{3+} on one sublattice, which we will henceforth refer to as the up sublattice, exhibits a nearly linear increase with the field. The splitting for down-sublattice Er^{3+}, on the other hand, first decreases to a minimum, amounting to 0.90 ± 0.02 cm^{-1}, at a field of 0.88 ± 0.03 T. Also derived from line separations such as in Fig. 2 is the Zeeman splitting of the $^4I_{15/2}(1)$ ground-state doublet. The results, given in the lower frame of Fig. 3, are seen to behave quite similarly. Here, Δ for the down sublattice reaches a minimum of 0.33 ± 0.07 cm^{-1} at 0.52 ± 0.03 T.

The very occurrence of a finite minimum provides evidence for the internal field to contain a perpendicular component, i.e., from the magnetic point of view the Er^{3+} centers are, as opposed to the Mn^{2+}, not located on sites of tetragonal symmetry. This is further established by similar experiments conducted in fields directed along the [110] and [100] axes, not presented in detail here. In these cases, each line of the Zeeman-split pattern of Fig. 1(a) is observed to quadruple, whereas all Er^{3+} would have been equivalent in the case of tetragonal symmetry. For arbitrary directions of the field, each line is seen to split in up to eight lines. These findings are not reconcilable with the earlier suggestion[2] that the charge compensation associated with the substitution of Er^{3+} for Mn^{2+} would be of delocalized nature. Instead, the results are indicative of the formation of a single kind of center,

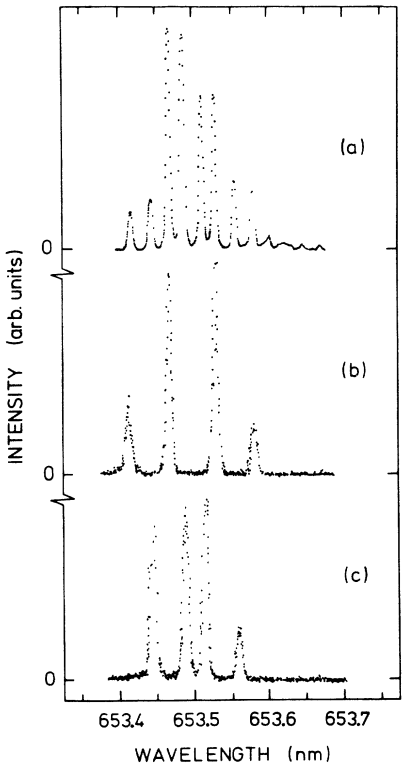

FIG. 2. Luminescence spectra of the $^4F_{9/2}(1)$-$^4I_{15/2}(1)$ transition in a magnetic field of 0.3 T along [001]: (a) excitation of Er^{3+} on both sublattices at 514 nm: (b) selective excitation of $^4F_{9/2}(1)_+$ of Er^{3+} on the up sublattice; (c) same, but down sublattice.

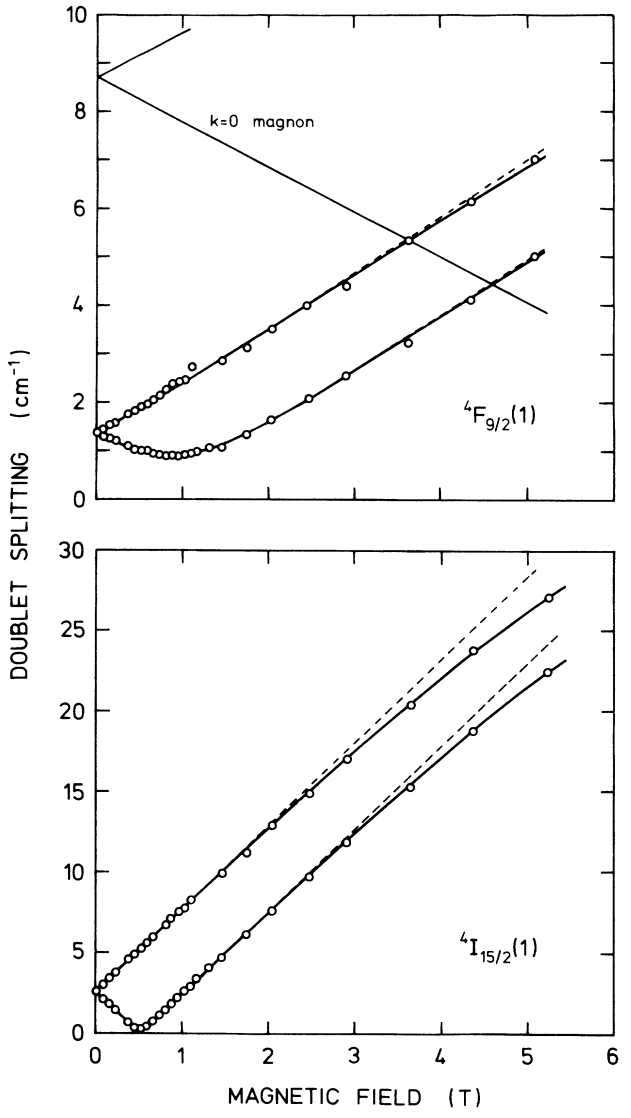

FIG. 3. Energy splittings of the $^4F_{9/2}(1)$ and $^4I_{15/2}(1)$ doublets in fields along [001]. Solid lines represent fits of Eq. (1). Dashed curves are as the solid curves, but with the quadratic Zeeman effect set to zero. The $^4F_{9/2}(1)$ splittings intersect the $k=0$ down-magnon branch.

breaking the local symmetry in the sense that the Er^{3+} magnetic moments point in eight distinct directions in compliance with the rutile structure. We note in this connection that the magnetic environment of the Mn^{2+} rotates over $\pi/2$ about the [001] axis when going from one sublattice to the other. This imposes an arrangement of the four up and four down sublattice Er^{3+} moments as depicted schematically in Fig. 4. Indeed, a detailed inspection of the experimental results in external fields canted from [001] show the Er^{3+} on the two sublattices to experience different transverse fields along [110]. Because of the dense packing of the rutile structure, interstitial F^- ions are unlikely. The assertion of a replacement of a neighboring F^- ion by residual O^{2-}, on the other hand, would explain the results. Furthermore, a consequence of the local symmetry breaking is that the principal axes of the g tensors of $^4F_{9/2}(1)$ and $^4I_{15/2}(1)$ are not directed along the crystal axes.

A quantitative description of the observed $^4F_{9/2}(1)$ and $^4I_{15/2}(1)$ splittings with field may be gained from a spin Hamiltonian of the form

$$\mathcal{H}=\mu_B \sum_{\alpha,\beta} g_{\alpha\beta} J_\alpha (\mathbf{H}+\mathbf{H}_i)_\beta + \mu_B^2 \sum_{\alpha,\beta,\gamma,\delta} G_{\alpha\beta\gamma\delta} J_\alpha J_\beta (\mathbf{H}+\mathbf{H}_i)_\gamma (\mathbf{H}+\mathbf{H}_i)_\delta , \quad (1)$$

appropriate to a manifold of constant J. Here, $\mathbf{H}$ is the external field, $\mathbf{H}_i=\mathbf{H}_{\rm dip}+[2(g_J-1)/g_J]\mathbf{H}_{\rm ex}$ is the internal field composed of dipolar and exchange parts, $g_{\alpha\beta}$ is the g tensor, and $G_{\alpha\beta\gamma\delta}$ is a fourth-rank tensor necessary to account for the quadratic Zeeman effect observed at higher fields. The indices α, β, γ, and δ run over x, y, and z. For both doublets we adopt an effective $J=\frac{1}{2}$. The energy splittings as derived from Eq. (1) at a fixed direction of $\mathbf{H}$ have the analytical form of the square root of a quartic polynomial in H, with the sign of H dependent on the sublattice. Least-squares adjustments of these expressions have been achieved to the measured field-dependent splittings of the excited doublet as well as those of the ground doublet. The field directions considered are [001], [100], and [110], and, to a lesser extent, [111] and [1$\bar{1}$1]. In all cases Eq. (1) turned out to provide an adequate description of the splittings up to the highest fields considered. As an example, the fits for $\mathbf{H}$ along [001] are represented in Fig. 3 as the solid lines. To demonstrate the size of the second-order Zeeman effect, also inserted in Fig. 3, as the dashed lines, are the dependencies recalculated from Eq. (1) with the part quadratic in the field set to zero. At 5 T, these parts are thus seen to contribute by about 0.1 cm^{-1} for $^4F_{9/2}(1)$, and 1.5 cm^{-1} for $^4I_{15/2}(1)$. In general, the quadratic Zeeman effect is stronger in the case of the ground state, and reaches a maximum for $\mathbf{H}$ parallel to [001], but even then it is negligible below 2 T. Finally, with a detailed analysis of the fitted results for the various directions of the field, the coefficients $\mu_{\alpha\beta}$ of the leading part of the energy splitting,

$$\Delta=\mu_B \left[\sum_{\alpha,\beta} \mu_{\alpha\beta}(\mathbf{H}+\mathbf{H}_i)_\alpha (\mathbf{H}+\mathbf{H}_i)_\beta\right]^{1/2} , \quad (2)$$

where $\mu_{\alpha\beta}=\sum_\gamma g_{\alpha\gamma} g_{\gamma\beta}$, as well as the internal fields $\mathbf{H}_i$ have been extracted. The results are summarized in Table I both for the $^4F_{9/2}(1)$ and $^4I_{15/2}(1)$ doublets.

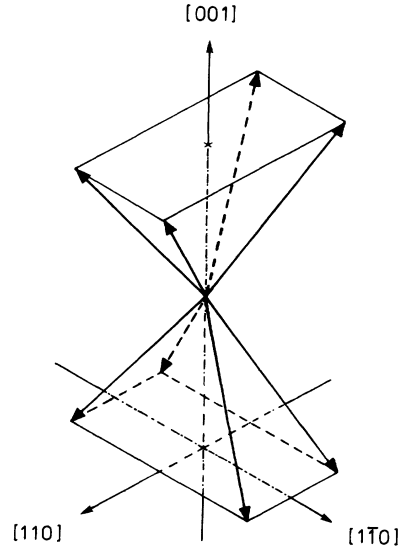

FIG. 4. Schematic representation of the eight directions the Er^{3+} moments assume in MnF_2.

IV. GENERATION OF RESONANT MAGNONS

As already pointed out, the method of observing a generation of magnons following excitation of the upper doublet state $^4F_{9/2}(1)_+$ is to see the decay to $^4F_{9/2}(1)_-$ accelerate when the doublet splitting surpasses the magnon energy gap. The latter is known to spread over about 0.07 cm^{-1} because of dipolar interactions.[6] Also given in the upper panel of Fig. 3 are the lowest $k=0$ energies of the two magnon branches as they develop in external fields along [001] according to the relation

$$\varepsilon_{k=0}=\varepsilon_{k=0}(H=0)\pm g\mu_B H . \quad (3)$$

Here $\varepsilon_{k=0}(H=0)=g\mu_B(2H_E H_A+H_A^2)^{1/2}$, in which $g\approx 2$, and H_E and H_A are fields representing the exchange and anisotropy, respectively. Near 0 K we have $g\mu_B H_E=48.8$ cm^{-1}, $g\mu_B H_A=0.78$ cm^{-1}, and $\varepsilon_{k=0}(H=0)=8.71\pm0.04$ cm^{-1}.[7-10] From a comparison

TABLE I. Splitting coefficients $\mu_{\alpha\beta}$ and internal fields $H_i^{(\alpha)}$ of Er^{3+} in excited and ground doublets with reference to the crystalline axes.

	$^4F_{9/2}(1)$	$^4I_{15/2}(1)$
μ_{xx}	34.9±0.2	43.9±0.2
μ_{yy}	22.83±0.19	31.0±0.2
μ_{zz}	6.54±0.12	123.6±0.3
μ_{xy}	8.8±0.6	0.0±0.6
μ_{xz}	0±10	50±15
μ_{yz}	0±10	40±15
$H_i^{(x)}$ (T)	0.4±0.2	0.8±0.2
$H_i^{(y)}$ (T)	0.2±0.1	0.8±0.2
$H_i^{(z)}$ (T)	0.8±0.2	0.0±0.2

of Eqs. (2) and (3), the $^4F_{9/2}(1)$ doublet separation and the magnon energy gap are found to intersect at a field of 3.58±0.05 T for Er^{3+} on the up sublattice, and at 4.56±0.05 T for Er^{3+} on the down sublattice. Note that only down magnons are to be generated in fields parallel to [001].

To measure the decay rates, the luminescence arising from $^4F_{9/2}(1)_-$ has been followed as a function of time. As is exemplified in Fig. 5, the luminescence exhibits at short times the increase associated with the relaxation, but ultimately decays with the return of the excited populations back to $^4F_{15/2}$. A detailed analysis of the data indeed bears this out, with the exception of the regime close to intersection as well as beyond this point in the case of high pumping powers, the luminescent intensity $I(t)$ is faithfully described by a single-exponential rise in parallel with a long-time decay. That is,

$$I(t)=I(0)[1-\exp(-t/T_{\text{eff}})]\exp(-t/\tau_R)\ , \qquad (4)$$

where T_{eff} is an effective relaxation time connecting the $^4F_{9/2}(1)$ states, and τ_R is the time against decay out of the $^4F_{9/2}(1)$ doublet, either directly by luminescence or by multiphonon processes involving $^4I_{9/2}$, located about 2800 cm^{-1} below $^4F_{9/2}(1)$, as intermediary.[11] The fits yield $\tau_R=235\pm10$ μs in zero field, weakly diminishing with the field to 195±10 μs at 3.5 T.

In Fig. 6 the results for T_{eff} of both up- and down-sublattice Er^{3+} are presented as a function of a magnetic field parallel to [001]. The time T_{eff} is seen to stay nearly level at first, and then to decrease gradually until a sudden drop is observed. This drop which covers over an order of magnitude within a field increment of 0.2 T only, occurs around 3.60±0.03 T for up-sublattice Er^{3+} and 4.60±0.05 T for down-sublattice Er^{3+}, the very points at which the $^4F_{9/2}(1)$ level separation crosses the magnon gap. For the up-sublattice Er^{3+} this is shown to better advantage in the inset of Fig. 6.

To expose the breakaway at the intersection points more clearly, we consider the field dependence of the relaxation of Er^{3+} by phonons in somewhat greater detail. At temperatures so low that thermal Raman and Orbach processes are frozen out, the phonon-associated relaxation within $^4F_{9/2}(1)$ is governed by direct processes, i.e., the energy emitted by the spin system is taken up by a resonant phonon, or vice versa. For Kramers doublets, direct spin-phonon relaxation is only operative through admixture of other levels by the magnetic field breaking the Kramers symmetry. In paramagnetic systems this results in a fifth-power dependence of the direct spontaneous relaxation rate T_1^{-1} on the field,[12,13] as opposed to a third-power dependence for nonconjugated levels.[14] The present case is somewhat more complicated in that the admixing is additionally induced by the internal field, leading to

$$T_1^{-1}=C\Delta^3\left[\sum_{\alpha,\beta}\lambda_{\alpha\beta}(\mathbf{H}+\mathbf{H}_i)_\alpha(\mathbf{H}+\mathbf{H}_i)_\beta\right]\ , \qquad (5)$$

where $\lambda_{\alpha\beta}$ is a second-rank tensor containing the admixing. Further, the low-field plateau is observed to be weakly dependent on the laser intensity, presumably because of Raman and Orbach processes invoked by high-frequency nonthermal phonons generated in the nonradiative decay out of $^4F_{9/2}(1)$. The rate T_{eff}^{-1} actually observed, therefore, is made up of $(1+2p_0)/T_1$, with p_0 the thermal occupation number of the resonant phonon modes, in parallel with a residual field-independent rate. Note that p_0 reaches a value of about 0.6 at the minimum splitting and 1.5 K. Simultaneous adjustments of T_{eff} pertaining to the two sublattices have been accomplished to all data below the intersection points. Here, use has been made of the Δ's deduced in Sec. III. The results of the fitting are represented by the solid lines in Fig. 6. The

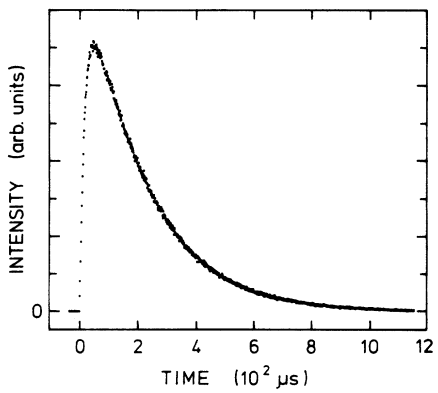

FIG. 5. Development with time of the luminescent intensity from $^4F_{9/2}(1)_-$ following pulsed optical population of $^4F_{9/2}(1)_+$ at 1.5 K and zero magnetic field.

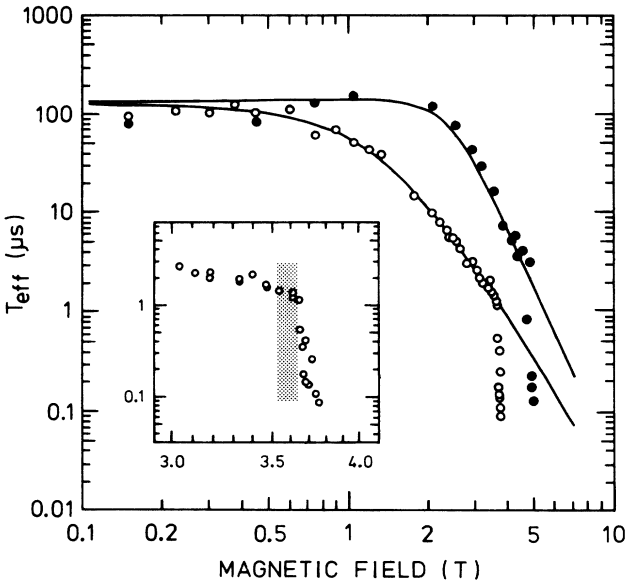

FIG. 6. Relaxation time within $^4F_{9/2}(1)$ of Er^{3+} on the up (open circles) and down (solid circles) sublattices vs a field along [001]. Solid lines represent a fit based on Eq. (5) to the data below intersection with the down-magnon branch. In the inset, the regime of significant non-single-exponentiality is indicated for up-sublattice Er^{3+}, where data points refer to the phonon part of the decay.

minor deviations at low fields are presumably caused by the coincidence of the optical transitions of Er^{3+} on the two sublattices, increasing the effective concentration of excited Er^{3+}, and thus the number of phonons generated in the optical pumping. The important point advanced by these fits, however, is that beyond the intersections the $T_{\rm eff}$ data distinctly deviate from the phonon-only $T_{\rm eff}$, unambiguously confirming generation of magnons by decay of Er^{3+} within $^4F_{9/2}(1)$ to take place.

It has already been discussed that in fields along [110], four inequivalent classes of Er^{3+} sites arise. The $^4F_{9/2}(1)$ Zeeman splitting of the Er^{3+} having the highest-energy $^4F_{9/2}(1)_-$-$^4I_{15/2}(1)_-$ transition is followed as a function of field in Fig. 7. The splitting factor in this direction is so high as to make the crossing of the $^4F_{9/2}(1)$ splitting with the magnon branches feasible despite the fact that magnon energies do not come down with the field. In a field perpendicular to the [001] easy axis, the lowest $k=0$ magnon energies in fact become

$$\varepsilon_{k=0}=\{\varepsilon_{k=0}^2(H=0)+\tfrac{1}{2}g^2\mu_B^2H^2[1\pm(1+H_A/H_E)]\}^{1/2}\ . \tag{6}$$

Equation (6) has been derived from the classical equations of motion of the two sublattices magnetizations,[15] and is correct up to order H^3. The lowest intersection point is predicted by Eq. (6) to occur at a splitting of 8.7 cm^{-1}. The reduction of the relaxation time within $^4F_{9/2}(1)$ in a field along [110], presented in Fig. 8 as a function of the doublet separation, is observed to behave in a way essentially equal to the course in fields along [001]. The straight line in Fig. 8 represents the fifth-power dependence on Δ to which the phonon part of $T_{\rm eff}^{-1}$ approaches at fields substantially above H_i [cf. Eq. (5)]. The relaxation rate, however, increases sharply beyond a doublet separation of 8.9 ± 0.1 cm^{-1}, the point at which within the uncertainties Δ matches $\varepsilon_{k=0}$ in perpendicular fields.

To conclude this section, we consider in more detail

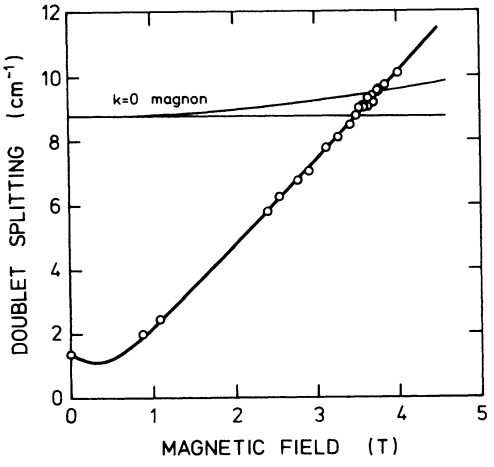

FIG. 7. Energy splitting of $^4F_{9/2}(1)$ of Er^{3+} with the highest-energy $^4F_{9/2}(1)_-$-$^4I_{15/2}(1)_-$ transition in a field along [110]. Solid curve is the fit of Eq. (1). Also inserted is the field dependence of the $k=0$ magnon energies according to Eq. (7).

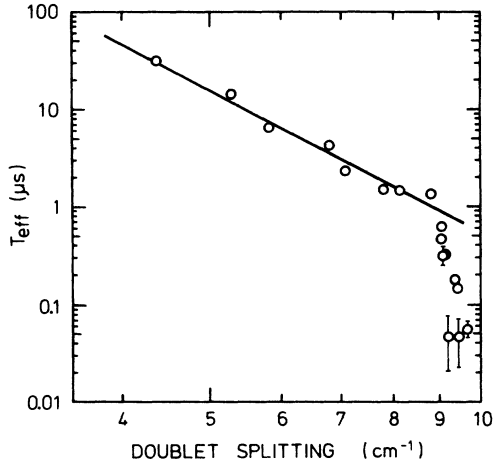

FIG. 8. Relaxation time within $^4F_{9/2}(1)$ vs the doublet splitting in a field along [110]. Solid line reflects the fifth-power dependence of $T_{\rm eff}^{-1}$ on H below intersection.

the relaxation among the $^4F_{9/2}(1)$ levels in fields close to the intersection. Time evolutions of the luminescent intensities just below, precisely at, and just above the intersection are presented in Fig. 9 for fields parallel to [001]. Both in the regime of relaxation by phonons only and the regime of relaxation predominantly by magnons, the increase of the $^4F_{9/2}(1)_-$ luminescence is single exponential. In the vicinity of the intersection, however, the increase turns out to contain fast as well as slow components. The reach of the deviations from single exponentiality is about 0.05 T at either side of the intersec-

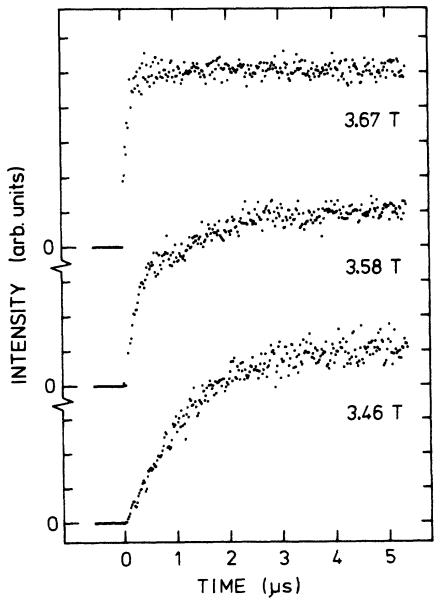

FIG. 9. Evolution with time of the $^4F_{9/2}(1)_-$ luminescent intensity following excitation into $^4F_{9/2}(1)_+$ just below (3.46 T), precisely at (3.58 T), and just above (3.67 T) intersection for the up-sublattice Er^{3+}. The field is aligned along [001].

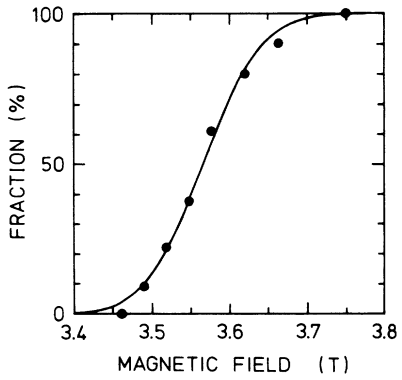

FIG. 10. Fraction of the fast decay among the $^4F_{9/2}(1)$ levels for up-sublattice Er^{3+} vs a field along [001]. Solid line represents an adjustment under the assumption of a Gaussian profile.

tion, as is indicated in the inset of Fig. 6. It is reasonable to conjecture that the $^4F_{9/2}(1)$ doublet separation is inhomogeneously broadened. The fast components thus originate from those excited Er^{3+} whose separations already match a magnon energy, whereas the slow components arise from excited Er^{3+} relaxing by phonons only. The fraction of the intensity rise associated with the fast components, as derived from data such as those in Fig. 9, is given in Fig. 10 as a function of the field. Here, for simplicity, the rise is represented by a sum of a fast and a slow exponential on the grounds that the relaxation by magnons is so much faster than relaxation by phonons. The gradual taking over by the fast components on traversing the inhomogeneous broadening then appears to be quantifiable with the function

$$\tfrac{1}{2}\{1+\mathrm{erf}[g\mu_B(H-H_{\mathrm{center}})/(2\ln 2)^{1/2}\Gamma]\} ,$$

which describes a shifting of weights under the assumption of a Gaussian profile. The full width at half maximum Γ has been adjusted to the data of Fig. 10, to yield $\Gamma=0.19\pm0.04$ cm^{-1}. A minor part of Γ may arise from the dipolar spread of the magnon dispersion.

V. MAGNON BOTTLENECK

The optically excited two-level scheme utilized above for the generation of monochromatic magnons further is capable of detecting magnons through capture by Er^{3+} in the $^4F_{9/2}(1)_-$ state. Here, we focus on the detection of magnons generated in the decay following optical excitation under bottlenecking conditions. Magnons then raise Er^{3+} back to $^4F_{9/2}(1)_+$ because a magnon is, on the average, reabsorbed by an excited Er^{3+} prior to their decay by thermalization or, for that matter, escape out of the excited zone. The degree of bottlenecking depends, of course, on N^*, the concentration of excited Er^{3+}. Note that the metastable Er^{3+} remain in $^4F_{9/2}(1)_-$ for a time τ_R, 3 orders of magnitude longer than it takes to decay spontaneously from $^4F_{9/2}(1)_+$.

A means to observe the occurrence of a bottleneck is to examine the associated slowing down of the relaxation among the $^4F_{9/2}(1)$ levels once the $^4F_{9/2}(1)_+$ population N_+ has, to some degree, fallen below the $^4F_{9/2}(1)_-$ population N_-. In the regime where N_+ still exceeds N_-, on the other hand, bottlenecking leads to an acceleration of the decay because of stimulated emission. A representative example of the increase of the $^4F_{9/2}(1)_-$ luminescent intensity upon severe optical pumping is given in Fig. 11. Here, the field is along [110] and above the intersection. As opposed to the low-intensity case (cf. upper trace of Fig. 9), the acceleration turns into a slowing down around $N_+\approx N_-$. It is noted that the depopulation of $^4F_{9/2}(1)_+$, as measured via its luminescence, is found to be precisely complementary to the rise of $^4F_{9/2}(1)_-$. This point is of relevance in that it evidences predominance of the processes within $^4F_{9/2}(1)$. It is further noted that the phonons are not yet bottlenecked at the laser powers used. This has been verified from the absence of any N^* dependence of T_{eff} in fields below the intersection point.

The decays have been quantitatively analyzed in terms of phenomenological rate equations governing the populations N_+ and N_- of the $^4F_{9/2}(1)$ levels as well as the occupation number m of the resonant magnon modes. These equations may be written as

$$\begin{aligned}
\frac{dN_+}{dt} &= -\frac{(1+m)N_+ - mN_-}{T_{1m}} \\
&\quad -\frac{(1+p_0)N_+ - p_0N_-}{T_{1p}} - \frac{N_+}{\tau_R} + \phi(t) , \\
\frac{dN_-}{dt} &= \frac{(1+m)N_+ - mN_-}{T_{1m}} \\
&\quad +\frac{(1+p_0)N_+ - p_0N_-}{T_{1p}} - \frac{N_-}{\tau_R} , \\
\frac{dm}{dt} &= \frac{(1+m)N_+ - mN_-}{D(\omega)\,\Delta\omega\,T_{1m}} - \frac{m-m_0}{\tau_m} ,
\end{aligned} \tag{7}$$

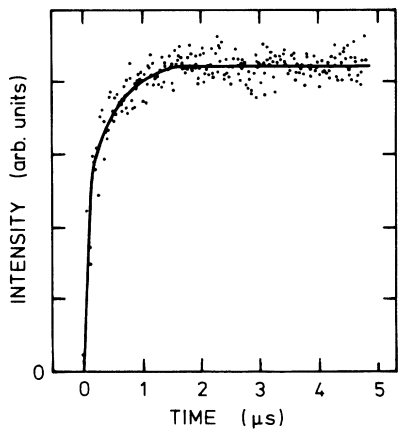

FIG. 11. Evolution with time of the $^4F_{9/2}(1)_-$ luminescent intensity in a field of 3.67 T along [110] for the highest N^* attained ($N^*\approx 5\times10^{17}$ cm^{-3}). The increase of the $^4F_{9/2}(1)_-$ population markedly slows down, indicative of bottlenecking of magnons. Solid line represents a numerical solution of Eqs. (7).

in which T_{1m} and T_{1p} denote the spontaneous direct spin-magnon and spin-phonon relaxation times, $D(\omega)\Delta\omega$ is the number of magnon modes resonant with the spin transition having a width $\Delta\omega$ in the angular frequency ω, τ_m is the average time of removal of the magnons, and m_0 and p_0 are the thermal occupation numbers. Note that at the intersection m_0 and p_0 are of order 10^{-4} at 1.5 K. Feeding by optical pumping is restricted to the upper level through the function $\phi(t)$, where $\int_0^\infty \phi(t)dt = N^*$ is the total number of Er^{3+} centers excited by the laser pulse. Radiative decay is included for completeness, its effects being entirely negligible on the time scales of interest here. In the event of high pumping, the major terms in Eq. (7) are those involving multiple emission and reabsorption of magnons by the Er^{3+}. At first, the decay of ${}^4F_{9/2}(1)_+$ to ${}^4F_{9/2}(1)_-$ becomes accelerated through stimulated emission of magnons, growing with m until emission and reabsorption balance, i.e., $(1+m)N_+ \approx mN_-$. From there on, the decay slows down as a result of the bottlenecking.

Equations (7) have been solved numerically over the full range of N_- under bottlenecking conditions. Subsequently, adjustments to coincidence with the observed temporal evolutions of N_- have been achieved. An example of these adjustments, for the highest bottlenecking attained, is given as the solid line in Fig. 11. When the majority of the excited Er^{3+} are relaxed to ${}^4F_{9/2}(1)_-$, the decay becomes virtually single exponential with an effective relaxation time

$$T_{\text{eff}} = [(1+2m_0)/(1+\sigma)T_{1m} + (1+2p_0)/T_{1p}]^{-1} , \quad (8)$$

where the degree of bottlenecking is appropriately expressed by the bottlenecking factor

$$\sigma = N^*\tau_m / D(\omega)\Delta\omega T_{1m} , \quad (9)$$

i.e., the ratio of the rate with which magnons of a particular mode are scattered off the Er^{3+} spin system, $N^*/D(\omega)\Delta\omega T_{1m}$, over the damping rate τ_m^{-1}. In the case of vanishing N^* ($\sigma \ll 1$), the decay of N_+ following the exciting pulse is, according to Eqs. (7), strictly single exponential over its full span, with a time constant still given by Eq. (8).

Effective relaxation times pertaining to the final portions of the decays such as in Fig. 11 are presented in Fig. 12 as a function of N^* for $\omega = 9.5\pm0.1$ cm^{-1}, corresponding to k's about 5% out into the zone. Here, the N^* scale is taken proportional to the luminescent intensity, while its absolute calibration has been extracted, to an accuracy of 20%, from separate experiments on the absorption of the laser light by the crystal. As is apparent from Eq. (8), the combination of quantities provided by T_{eff} after removal of the phonon part is $(1+\sigma)T_{1m}$. Upon substituting $T_{1p} = 0.8\pm0.2$ μs, obtained from extrapolation of the relaxation times below the intersection point [cf. Fig. 8], T_{eff} at the maximum $N^* = (5\pm1)\times10^{17}$ cm^{-3} thus yields $(1+\sigma)T_{1m} = 1.4\pm0.3$ μs. The time T_{1m} is best estimated from extrapolation to very low laser powers, where, as has already been noted, the decays are single exponential over the entire range of N_-. The

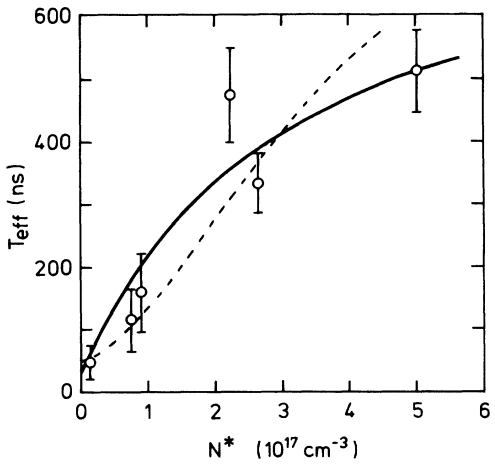

FIG. 12. Dependence of T_{eff} on N^* beyond $N_+ \approx N_-$. Curves represent calculated dependences of T_{eff} based on Eqs. (8) and (9) on the assumption of a constant magnon lifetime τ_m (solid curve) or a τ_m proportional to N^* (dashed curve).

quantity T_{eff} recalculated from Eqs. (8) and (9) with, for the moment, constancy of τ_m is inserted in Fig. 12 as the solid curve, to find a satisfactory reproduction of the course of the experimental T_{eff} versus N^*. The spin-magnon relaxation time is found to amount to $T_{1m} = 30\pm15$ ns, so that $\sigma \approx 45$ at the maximum N^*. The agreement also establishes the adequacy of the simple model underlying Eqs. (7) for the present purpose.

The results for T_{1m} and σ just arrived at from the N^* dependence of T_{eff} allow, by the use of Eq. (9), an estimation of a quantity of primary interest, the magnon lifetime τ_m. In the quadratic approximation of the magnon dispersion, the density of magnon states is, per branch,

$$D(\omega) = (4N/\pi^2)[\omega(\omega^2-\omega_0^2)^{1/2}/\omega_E^3] , \quad (10)$$

in which ω_0 corresponds to the energy gap at the intersection point, ω is the angular frequency of the resonant magnons, $\omega_E = 2\mu_B H_E$, and N is the number magnetic unit cells per cm^{-3}. Using $\omega_0 = 8.9\pm0.1$ cm^{-1} and $\omega = 9.5\pm0.1$ cm^{-1}, we find $D(\omega) = 7.4\times10^6$ cm^{-3}s. We further set the width of the spin transition $\Delta\omega$ equal to Γ as obtained from the behavior of the decay in the passage through the intersection (Sec. IV), yielding $\Delta\omega = 3.6\times10^{10}$ s^{-1}. Insertion of these values in Eq. (9) then leads to $\tau_m = 0.7$ μs at the maximum N^*.

To interpret this result, we note that the time after which a magnon emitted by an excited Er^{3+} is interrupted by reabsorption by another excited Er^{3+} equals $T_{\text{int}} = D(\omega)\Delta\omega T_{1m}/N^*$. At the maximum N^*, therefore, $T_{\text{int}} = 16$ ns. This corresponds to a mean free distance of $\Lambda = v_g T_{\text{int}} \approx 11$ μm, given that the group velocity in the Debye approximation,

$$v_g = \tfrac{1}{2}a^{2/3}c^{1/3}\omega_E[1-(\omega_0/\omega)^2]^{1/2} , \quad (11)$$

amounts to 700 ms^{-1} at the relevant wave vector. In order to distinguish between magnon decay by escape out of the excited zone and decay by processes intrinsic to the magnon system itself, we compare the mean distance

covered by a magnon prior to its removal by spatial diffusion, $\Lambda\sigma^{1/2}$, with the typical distance to the surface of the excited zone, an estimate of which is the radius R of the laser beam. We have $\Lambda\sigma^{1/2}\approx 75$ μm at the maximum N^*, while $R\approx 100$ μm. It thus appears that escape out of the zone is significant, and that, by the same argument, the τ_m found constitutes a lower limit for intrinsic decay mechanisms.

It should finally be pointed out that spatial diffusion implies that τ_m is dependent on N^*, contrary to the assumptions made in calculating the solid curve in Fig. 12. In the case of predominance of spatial diffusion, τ_m is proportional to N^*, and σ thus varies with $(N^*)^2$.[16] The development of $T_{\rm eff}$ with increasing N^* inclusive of the phonon part would then follow the dashed curve in Fig. 12, which has been drawn for $T_{1m}=40\pm 15$ ns and $\sigma=50$ at the maximum N^*. The real situation is likely to be somewhere intermediate between the two extreme cases worked out. This does however not detract from the conclusion that the magnon decay is inherently weak, with τ_m's of order 1 μs. This result is reconcilable with experiments conducted closer to the zone center. Antiferromagnetic resonance[9] and parallel pumping[17] in MnF_2 have yielded decay times of order 10 μs at 2 K, despite the fact that these techniques probe elastic scattering as well.

VI. CONCLUDING REMARKS

We have demonstrated that optically excited centers may act as energy-selective magnon generators. In the antiferromagnet MnF_2, magnons have in this way been produced in the direct decay within the $^4F_{9/2}(1)$ Kramers doublet of Er^{3+} to the extent that magnon occupations substantially above thermal equilibrium have been attained. We have further examined the Zeeman effect of the $^4F_{9/2}(1)-{}^4I_{15/2}(1)$ transition, to find the doublet separations and the magnetic orientations.

The scheme of optical generation, in principle, makes the entire Brillouin zone amenable to examination. In the present case, wave vectors have been selected in a range extending many times farther than what has been achieved with resonance techniques, like parallel pumping. The upper bound of $\mathbf{k}$ could be increased further in fields higher than the ones used here, notably fields transverse to the easy axis. More important, however, the optical scheme is straightforwardly adaptable to other magnetic systems, including ferromagnets, and other centers provided the magnon-phonon interaction is not too large. Coverage of the entire Brillouin zone, permitting a comprehensive study of magnon damping as a function of wave vector, would come within reach in systems having a more narrow spin-wave band. A salient feature of a two-level optically excited system further is that conversely, when maintained in its lower state, it has the prospect of serving as a frequency-selective detector for magnons supplied by an external source. The detection is most sensitive under the conditions of bottlenecking, such as reached in the present system. The magnon occupation number then is directly reflected in the ratio of the luminescent intensities emitted by the doublet. For the relaxation by phonons not to interfere, however, the magnon bottlenecking factor should not exceed a few times T_{1p}/T_{1m}, which in the present case is of order 50. In regards to the frequency resolution, it is determined by the inhomogeneous width of the transition, but smaller bandwidths are likely to be achievable means of a hole burning and fluorescence line narrowing.

A feature making the optical schemes particularly valuable for investigations of magnon dynamics is that the concentration of the scattering centers and the geometry of their volume of confinement may, in a single experiment and under otherwise identical conditions, be varied over a wide range via the intensity and diameter of the laser beam. This permits to discriminate between the removal of nonequilibrium magnons by, on the one hand, intrinsic decay processes and, on the other hand, ballistic escape and spatial diffusion to the nonpumped regions of the specimen. The bottleneck experiments conducted here indicate that imprisoned magnons in MnF_2 escape spatially from the excited zone to a significant degree when the group velocity allows them to do so.

Finally, it is of interest to consider the conditions under which intrinsic magnon decay is measured rather than ballistic or diffusive escape. This requires, as already noted, that $\Lambda\sigma^{1/2}\ll R$. Upon writing out the N^* and R dependencies explicitly, this condition may alternatively by written $v_g^2 D(\omega)\Delta\omega T_{1m}\tau_m \ll N^* R^2$.[18] Accordingly, measurement of the intrinsic τ_m becomes feasible upon sufficiently increasing the diameter of the excited zone, but not merely by expanding the laser beam at constant power, which would correspond to constant N^*R^2. Increase of the laser power at constant R is another option as long as σ does not grow too far above T_{1p}/T_{1m}. It is also clear that the condition is the easier met the higher the temperature because τ_m for intrinsic decay would diminish.

ACKNOWLEDGMENTS

The authors thank C. R. de Kok for technical assistance. The work was made possible by a grant from the Netherlands Foundation Janivo, and further was supported financially by the Netherlands Foundations Fundamenteel Onderzoek der Materie (FOM) and Zuiver Wetenschappelijk Onderzoek (ZWO).

---

[1]A preliminary account has been presented in G. J. Jongerden, A. J. Kil, J. I. Dijkhuis, A. F. M. Arts, and H. W. de Wijn, J. Phys. (Paris) Colloq. **46**, C7-241 (1985).

[2]Luminescence spectra in zero field have been reported by B. A. Wilson, W. M. Yen, J. Hegarty, and G. F. Imbusch, Phys. Rev. B **19**, 4238 (1979).

[3]Optical generation and bottlenecking of phonons was accomplished in J. I. Dijkhuis, A. van der Pol, and H. W. de Wijn,

Phys. Rev. Lett. **37**, 1554 (1976), and optical detection of phonons by imprisonment in K. F. Renk and J. Deisenhofer, Phys. Rev. Lett. **26**, 764 (1971).

[4]A. A. Kaplyanskii and S. Basun, in *Nonequilibrium Phonons in Nonmetallic Crystals, Modern Problems in Condensed Matter Sciences,* edited by W. Eisenmenger and A. A. Kaplyanskii (North-Holland, Amsterdam, 1986), Vol. 16, Chap. 8.

[5]P. A. M. Berdowski, M. J. J. Lammers, and G. Blasse, J. Chem. Phys. **83**, 476 (1985).

[6]R. Loudon and P. Pincus, Phys. Rev. **132**, 673 (1963); A. Brooks Harris, Phys. Rev. **143**, 353 (1964).

[7]F. M. Johnson and A. H. Nethercot, Jr., Phys. Rev. **114**, 705 (1959).

[8]C. Trapp and J. W. Stout, Phys. Rev. Lett. **10**, 157 (1963).

[9]J. P. Kotthaus and V. Jaccarino, Phys. Rev. Lett. **28**, 1649 (1972).

[10]F. Keffer, in *Encyclopedia of Physics,* edited by S. Flügge (Springer, New York, 1966), Vol. XVIII/2, p. 1 ff.

[11]M. J. Weber, Phys. Rev. B **8**, 54 (1973); J. M. Flaherty and B. di Bartolo, J. Lumin. **8**, 51 (1973).

[12]J. I. Dijkhuis, K. Huibregtse, and H. W. de Wijn, Phys. Rev. B **20**, 1835 (1979).

[13]H. Wolfrum, K. Lanzinger, and K. F. Renk, Opt. Lett. **5**, 294 (1980).

[14]A. Abragam and B. Bleaney, *Electron Paramagnetic Resonance of Transition Ions* (Oxford University Press, London, 1970), Chap. 10.

[15]F. Keffer and C. Kittel, Phys. Rev. **85**, 329 (1952).

[16]J. I. Dijkhuis and H. W. de Wijn, Phys. Rev. B **20**, 1844 (1979).

[17]J. Barak, S. M. Rezende, A. R. King, and V. Jaccarino, Phys. Rev. B **21**, 3015 (1980).

[18]The phonon counterpart of this condition is treated in greater detail in Ref. 16.